On-line WAXD / SAXS Measurement for CO_2 Laser-Heated-Drawing of Poly(ethylene terephthalate) Fiber

TAKAYOSHI YAMAGUCHI[1], KOHEI KOMORIYAMA[2], YUTAKA OHKOSHI[1], HIROSHI URAKAWA[2], YASUO GOTOH[1], NORIHISA TERASAWA[2], MASANOBU NAGURA[1], and KANJI KAJIWARA[3]

[1]Faculty of Textile Science and Technology, Shinshu University,
3-15-1, Tokida, Ueda, Nagano, 386-8567, Japan
[2]Faculty of Engineering and Design, Kyoto Institute of Technology,
Goshokaidoucho, Matsugasaki, Sakyo-ku, Kyoto, 606-8585 Japan
[3]Faculty of Home Economics, Otsuma Women's University
12, Sanbancho, Chiyoda-ku, Tokyo, 102-8357, Japan
Correspondence to: Y. Ohkoshi (E-mail: yokoshi@shinshu-u.ac.jp)

ABSTRACT: Fiber structure development in the poly(ethylene terephthalate) fiber drawing process was investigated by on-line measurement of wide-angle and small-angle x-ray scattering employing both a high-luminance x-ray source and a carbon dioxide laser-heated-drawing system. Intensity profile of transmitted x-ray confirmed the location of the neck-drawing point. Obtained diffraction images had a time-resolution of several milliseconds, which still leaves a great capacity for improvement. Crystal diffraction appeared in the wide-angle x-ray images almost instantaneously about 20 ms after necking, whereas a four-point SAXS pattern appeared immediately after necking. With the elapse of time after necking, the four-point scattering pattern changed to a meridional two-point shape.

KEYWORDS: X-ray diffraction, poly(ethylene terephthalate), fiber structure development, laser drawing, high-luminance X-ray source

INTRODUCTION

Neck-drawing, which is a kind of secondary drawing process, is an important process that determines structure and properties of synthetic fiber. It is a very complex process, in which fiber diameter changes rapidly, molecular chain aligns to the fiber axis, and the fiber structure is formed by orientation-induced crystallization within several milliseconds. Therefore, direct measurement in the vicinity of the neck-drawing point is required for quantitative analysis of the fiber-structure-development mechanism.

Reported studies on spinning-line measurement and drawing-line measurement fall into two categories: measurement of phenomenological parameters (diameter, temperature, etc.)[1-7,37,38], and x-ray diffraction measurement for direct observation of fiber structure development[8-36]. Studies falling under the former category have revealed that crystallization after necking causes a temperature increase[2,37]. Kikutani et. al. reported the development of molecular orientation before the neck-like deformation, which they analyzed by on-line birefringence measurement using a rotating polarizer[3]. Hirahata et al.'s study, falling under the latter category, reports observation of weak crystal reflections before neck-like deformation by wide-angle x-ray diffraction (WAXD) measurement for high-speed spin-line of PET fiber[10]. Samon and Schultz et al. measured both WAXD and small-angle x-ray scattering (SAXS) images simultaneously for the spinning process of polyamide 6, polyethylene, and poly (vinylyden fluoride) [14,15]. For the drawing process, most on-line measurement studies fall into one of two categories; batch drawing under small strain rate[20-32], and draw ratio dependence of continuous drawing[33-36]. In both cases, x-ray diffraction images are taken at a fixed position. In the former studies, structure development was measured at far smaller strain rates than those observed in the industrial process. In addition, the fiber structure development process is not analyzed by the latter category of studies. The results reported by Mahendrasingam et al.[21-25] are notable, because they reported x-ray diffraction images for the highest strain rate. They observed orientation-induced crystallization behavior by the images that were measured every 40 ms for a batch drawing process at strain rates of 0.01 to 15 s^{-1}, temperatures of 90 to 120°C, and draw ratios of 2.2 to 4.0. They then observed the onset of orientation-induced crystallization about 200 ms after 3.7 times drawing at 90°C under a strain rate

of 12.8 s^{-1}. However, this strain rate is about three orders of magnitude smaller than that applied in the continuous drawing process, and the draw ratio is almost the lowest draw ratio at which orientation-induced crystallization occurs. Because the orientation-induced crystallization rate increases with both draw ratio and drawing rate, we can speculate that they could not measure the orientation-induced crystallization behavior of drawing at the higher ratio or the higher strain rate by several decades of milliseconds time-resolution. Meanwhile, Wu et al. took WAXD/SAXS images 0.05 to 0.1 s after the pin-drawing point in the continuous drawing process of polyamide66[33], polypropylen[34] and poly (trimethylene terephthalate)[35,36] fiber. This method has a difficulty in measuring near the necking point, and also has a difficulty in application to high-speed drawing.

We succeeded in fixing neck-drawing point without contact by using CO_2 laser radiation, which can heat the running fiber rapidly and uniformly. Temperature and diameter profiles in the vicinity of neck-drawing point were measured by the procedure with high time-resolution[37,38]. The fiber structure development process was analyzed quantitatively within a time-resolution of 1 ms for PET from the temperature profiles measured by an IR thermometer[37], with a position resolution of 0.375 mm. We also analyzed drawing behavior, such as discontinuous change of the deformation form at a certain draw ratio, from the diameter profiles obtained by high-speed images of the neck-like deformation[38]. Additionally, we have analyzed fiber structure and mechanical properties of laser-heated drawn fibers.[39-44]

In this study, by applying both a CO_2 laser-heated-drawing system and a high luminance x-ray generation system, we investigated fiber structure development by taking WAXD/SAXS images for the neck-drawing process of PET fiber. We measured the transmitted x-ray intensity simultaneously in order to confirm the location of the neck-drawing point.

EXPERIMENTAL

Measuring system

Figure 1(a) shows a schematic diagram of the WAXD/SAXS measurement system, and figure 1(b) shows the CO_2 laser irradiation system as viewed along the fiber axis. Running fiber between feed and take-up roller was heated by the CO_2 laser irradiation, and then the heated fiber was drawn continuously to the ratio of feed speed to take-up speed. As shown in figure 1(a), we can take WAXD/SAXS images of the fiber in the drawing process. The *D* in figure 1(a) denotes the distance from CO_2 laser irradiation point to x-ray beam irradiation point. Both an x-ray beam and a CO_2 laser beam are radiated perpendicularly onto the running fiber in figure 1(b).

The x-ray generator used in this study was model FR-D of RIGAKU Electric Co., Ltd. Cu-Kα (0.154 nm wavelength) light was generated with a tube voltage of 45 kV and a tube current of 60 mA. The x-ray beam was converged by a side-by-side multilayer mirror system (Osmic Inc, USA, Confocal Max-Flux Optics). Then the x-ray beam, which has a diameter of about 0.8 mm, was radiated onto the running fiber. A 100-μm resolution, 1150×1150 pixel imaging plate (HR-V, Fuji Film Co., Ltd.) was exposed to the scattered x-ray beam, and then scanned by an R-AXIS-DS3 data reader. The obtained digital data were

stored and analyzed by computer. The WAXD images were taken at a camera length of 102 mm and an exposure time of 300 s, and the SAXS images were taken at a camera length of 615 mm and an exposure time of 600 s. In addition, transmitted x-ray intensity was monitored by a counter mounted in a vacuum chamber.

The CO_2 laser generator was Model PIN-20S manufactured by Onizuca Glass, Co., Ltd. (wavelength 10.6 μm). Beam diameter, which could be adjusted by a beam expander, was 2.6 mm. As shown in figure 1(b), the CO_2 laser beam was reflected by a mirror, and was radiated three times on the same point on the fiber. This multi-direction radiation enabled uniform heating of the fiber, even though it had a diameter in excess of 200 μm[38]. Irradiation from directions at uniform circumferential intervals is suggested for ideal uniform heating, but in this case, mirror interference restricts equatorial diffraction angle to less than 25 degrees. Therefore, in order to secure a measurable diffraction angle up to 40 degrees, mirror locations were determined such that the angles between the first incident beam, and the second and third beams were both 135 degrees.

Because the neck-drawing point moves with the laser irradiation point, the position of the optical unit can settle the *D* in figure 1 (a) by moving the optical unit shown in figure 1(b) parallel to the fiber-running direction. The optical unit was moved by a stepping-motor. The elapsed time from the necking to the x-ray irradiation can also be determined. Therefore, if the drawing process is sufficiently stationary, the fiber structure development process can be observed directly, by means of taking WAXD/SAXS images at various elapsed times after necking. We took both WAXD and SAXS images in succession at each measuring position *D* from –1.5 to +16.0 mm.

As mentioned below, the fiber-running location was set to the x-ray beam axis. The fiber-running line is prescribed by two ceramic thread guides that are mounted at the respective ends of the optical unit. The guide has a inside diameter of 1.0 mm, and the distance between guides is 188.5 mm. Straight wire having a diameter of 1.0 mm was installed between the thread guides, and the guide positions were adjusted in order to adapt the x-ray beam axis to the wire axis at both sides of the measuring region. The adjustment was repeated until the error became less than 0.1 mm. After the setting of the fiber running location, the change in the x-ray irradiation position when the optical unit is moved 1 mm is less than 1 μm.

The origin of the measuring position was adjusted by adapting the laser irradiation point to the x-ray irradiation point. The irradiation point of CO_2 laser beam, which was adjusted by a mirror, had an error of several hundred micrometers, because the setting was performed using a He-Ne guide laser under visual observation. In addition, the CO_2 laser beam has a diameter of 2.6 mm. Therefore, the CO_2 laser irradiation point could not be determined accurately. Therefore, we determined the neck-drawing point by the transmitted x-ray intensity measurement performed simultaneously with the SAXS imaging, and estimated the elapsed time after necking directly from the distance between the neck-drawing point and the x-ray irradiation point.

Material and Drawing Conditions

The as-spun fiber was prepared by the melt spinning of PET ([η]: intrinsic viscosity =0.945 dL/g; supplied from Toray, Co. Ltd.) by extrusion from a 1.0 mm diameter, one-hole spinneret at 290°C at a mass-flow

rate of 5.4 g/min and a take-up speed of 14.3 m/min. Extruded polymer was cooled by a water bath provided 0.15 m below the spinneret. The obtained monofilament has a diameter of 602 μm and a birefringence of 1.2×10^{-3}.

WAXD and SAXS images were measured for drawing of the as-spun monofilament under the following drawing conditions: draw ratio 4.5, laser power 5 W, and feed speed 1.0 m/min. The drawn fiber had a diameter of 288 μm and a birefringence of 0.177. WAXD and SAXS images were also taken for as-spun and drawn fibers. According to our previous work[37], temperature of 4.5 times drawn fiber takes the maximum of 157°C. Fiber structure and mechanical properties of the fiber obtained by similar drawing conditions have reported previously.[39, 40]

RESULTS AND DISCUSSION

Transmitted x-ray intensity

Figure 2 shows the transmitted x-ray intensity measured at each measuring point. The horizontal axis represents the distance *D*. The transmitted x-ray intensity shows a drastic increase about 1.5 mm after the laser beam irradiation point. The transmitted x-ray intensities before and after the position are 2.15×10^3 cps and 2.45×10^3 cps respectively, and the intensity without sample is 2.56×10^3 cps. The position should correspond to the neck-drawing point, because the ratio of attenuation rates before and after the point, 16% and 4%, corresponds to the ratio of fiber cross-section areas. We confirmed the neck-drawing point in this region by visual observation. The breadth of the intensity-changing region is about 1.2 mm. In view that the irradiated x-ray beam has a breadth of 0.8 mm and the neck-drawing region has a breadth of 0.1 mm[38], the fluctuation of neck-drawing point is not a dominant factor of the breadth.

A noteworthy feature of this measuring system is that we can determine the neck-drawing point from the transmitted x-ray intensity, because we can determine the distance from the neck-drawing point to the x-ray irradiation point directly with the same accuracy as fluctuation breadth of the neck-drawing point obtained WAXD/SAXS images were smeared by scattering from the fiber with fluctuations in elapsed time, which is determined by the fluctuation breadth. Accordingly, the elapsed time has an error determined by the fluctuation breadth of neck-drawing point and fiber-running speed. The above result indicates that the elapsed time for each x-ray diffraction images has an error of no more than ±8 ms. In order to optimize the drawing condition, fluctuation of the neck-drawing point can be controlled within ±0.1 mm, and the fiber-running speed can be elevated to more than ten times that employed in this study[38]. Therefore, this system should be able to obtain a resolution time of several μs.

WAXD Images

Obtained WAXD images are shown in Figure 3. The as-spun sample is revealed to be amorphous, because only an amorphous halo is observed in the image. The scattering concentrated at the equator appears just after necking. This indicates that only a part of amorphous phase is highly oriented. This scattering should be the same as that observed for PET film by Mahendrasingam *et al*.[20, 22-24] and Kawakami *et al*.[31, 32]

Crystal diffraction appeared abruptly 20 ms after necking. It is not observed at all in the 17 ms diffraction image, and becomes clear in the 30 ms image. The above result that these images are smeared within the corresponding elapsed time of less than 8 ms suggests the possibility that crystal diffraction appear almost instantaneously at 25-28 ms after necking. This result agreed with the reports by Kolb *et al.*[13] and Mahendrasingam.[23] that the crystallization occurred after the neck-like deformation. However, the crystallization time obtained in this study is far shorter than the crystallization time of 200 ms reported by Mahendrasingam.[23] The crystallization rate is almost 10 times that reported previously, probably due to the difference in drawing conditions; i.e., a drawing temperature about 100 K higher[37], a draw ratio 0.8 higher, and a strain rate 100 times as large. Accordingly, application of the measuring system used in this study enables direct analysis of the fiber structure development mechanism of a high-temperature, high-strain-rate, high-draw-ratio, and high-stress neck-drawing process. This analysis has higher practical value, because the drawing conditions are more similar to those used in industrial production.

Figure 4 shows diffraction intensity profiles along the equatorial and meridional directions. Each profile was obtained by background subtraction and smoothing. The as-spun profiles show an isotropic amorphous halo. The equatorial profiles show little intensity increase from the neck-drawing point. At 20 ms after necking, the amorphous halo vanishes, and instead obvious crystal diffraction peaks appear. Diffraction intensity increases gradually with elapsed time. In turn, because of the fiber temperature at 193 ms probably still higher than glass transition temperature[37], the decrease of peak width after 193 ms seems to be caused by the crystal melting and re-crystallization.

SAXS images

Figure 5 shows the obtained SAXS images. A remarkable finding is that four-point scattering already appeared from the neck-drawing point. That is prior to the clear appearance of crystal diffraction in WAXD image. This seems to indicate that some structure had been formed before the crystals were formed. The weak equatorial scattering appearing in the WAXD images is probably related to this structure.

The four-point scattering becomes clear with elapsed time after drawing, and seems to show a gradual change toward two-point shape. Figure 6 shows the intensity profiles along the q_e direction obtained by background subtraction and SAXS image integration from q_m=0.66 nm^{-1} to 1.19 nm^{-1}; $q = 4\pi\sin\theta/\lambda$. The value noted in this figure is the peak separation obtained by the peak fitting of three Gaussian peaks arranged symmetrically to the meridian. Because the change from four-point to two-point shape corresponds to the peak sharpening of WAXD profile, it seems to reflect development of lamella structure perpendicular to the fiber axis. The pattern changed toward meridional two-point shape with elapsed time after necking.

The equatorial streak appears after necking, and gradually increases in intensity with elapsed time. To clarify this trend quantitatively, Guinier plot of equatorial SAXS profiles is shown in figure 7. The integrated intensity profiles of $q_m = \pm$ 0.21 nm^{-1} were obtained by background subtraction. The intensity of the equatorial streak increased steeply about 13 ms after necking, and then it seems to saturate about 40 ms. Similar equatorial streak development was reported for polyethylene and poly (vinylidene fluoride) fibers

by Schultz et al[14, 15]. They suggested that the streak corresponds to the development of shish crystal, because it was vanished when the crystal reflection appeared[15]. In contrast with this study, the equatorial streak similarly appeared after necking, but did not vanish with crystallization.

CONCLUSIONS

By combining high-luminance x-ray source and laser-heated drawing, WAXD/SAXS images were obtained with a time resolution of several milliseconds. The time-resolution still leaves great capacity for improvement. Because location of the neck-drawing point is confirmed by transmitted x-ray intensity profile, elapsed time after necking can be determined accurately. The crystal reflection appears instantaneously in the WAXD image about 20 ms after necking, whereas the four-point pattern appears in the SAXS image immediately after necking. The four-point SAXS pattern became clear with elapsed time, and then the pattern changed toward the meridional two-point shape. When this measuring system is applied to various drawing conditions, the mechanism of fiber structure development can be analyzed quantitatively.

ACKNOWLEDGMENTS

The authors would like to express their gratitude to Toray. Co. for supplying material. This work was supported by a Grant-in-Aid for 21st COE Research by the Ministry of Education, Culture, Sports, Science and Technology of Japan, and also supported by Grants-in-Aid No.15350135 and No.15550182 by JSPS.

REFERENCES AND NOTES

1. Fujimoto, K.; Iohara, K.; Owaki, S.; Murase, Y. SEN'I GAKKAISHI, 1988, 44, 53.
2. Kikutani, T.; Kawahara, Y.; Matsui, T.; Takaku, A.; Shimizu, J. Seikei-Kakou 1989, 1, 333.
3. Kikutani, T.; Nakao, K.; Takarada, W.; Ito, H. Polym. Eng. Sci. 1999, 39, 2349.
4. Penning, J. P.; Ruiten, J. van; Brouwer, R.; Gabrielse, W. Polymer 2003, 44, 5869.
5. Rule, R. J.; MacKerron, D. H.; Mahendrasingam, A.; Martin, C.; Nye, T. M. W. Macromolecules 1995, 28, 8517.
6. Duchesne, C.; Kong, X.; Brisson, J.; Pesolet, M.; Prud'homme, R. E. Macromolecules 2002, 35, 8768.
7. Pellerin, C.; Prud'homme, R. E.; Pezolet, M.; Weinstock, B. A.; Griffiths, P R. Macromolecules 2003, 36, 4838.
8. Hsiao, B. S.; Barton Jr., R.; Quintana, J. J. Appl. Polym. Sci. 1996, 62, 2061.
9. Habrekorn, H.; Hahn, K.; Breuer, H.; Dorrer, H. D.; Matthies, P. J. Appl. Polym. Sci. 1993, 47, 1551.

10. Hirahata, H.; Seifert , S.; Zachamann, H. G. Polymer 1996, 37, 5131.
11. Samon, J. M.; Schultz, J. M.; WU, J.; HSIAO, B. S.; YEN, F.; Kolb, R. J. Polym. Sci. Part B 1999, 37, 1277.
12. Kolb, R.; Seifert, S.; Stribeck, N.; G. Zachmann, H. Polymer 2000, 41, 1497.
13. Kolb, R.; Seifert, S.; Stribeck, N.; G. Zachmann, H. Polymer 2000, 41, 2931.
14. Samon, J. Schultz, J. M. M. Macromolecules 1999, 32, 8121.
15. Schultz, J. M.; Hsiao, B. S.; Samon, J. M. Polymer 2000, 41, 8887.
16. Samon, J. M.; Schultz, J. M.; Hsiao, B. S.; Khot, S.; Johnson, H. R. Polymer 2001, 42, 1547.
17. Samon, J. M.; Schultz, J. M.; Hsiao, B. S. Polymer 2000, 41, 2169.
18. Hughes, D. J.; Mahendrasingam, A.; Oatway, W. B.; Heelley, E. L.; Martin, C.; Fuller, W. Polymer 1997, 38, 6427.
19. Hughes, D. J.; Mahendrasingam, A.; Martin, C.; Oatway, W. B.; Heelley, E. L.; Bingham, S. J.; Fuller, W. Review of Scientific Instruments. 1999, 70, 4051.
20. Blundell, D. J.; Mackerron, D. H.; Fuller, W.; Mahendrasingam, A.; Marian, C.; Oldman, R. Rule, R. J. J.; Riekel, C. Polymer 1996, 37, 3303.
21. Mahendrasingam, A.; Marian, C.; Fuller, W.; Blundell, D. J.; Oldman, R. J.; Harvie, J. L.; Mackerron, D. H.; Riekel, C.; Engstrom, P. Polymer 1999, 40, 5553.
22. Mahendrasingam, A.; Martin, C.; Fuller, W.; Blundell, D. J.; Oldman, R. J.; Mackerron, D. H.; Harvie, J. L.; Riekel, C. Polymer 2000, 41, 1217.
23. Blundell, D. J.; Mahendrasingam, A.; Marian, C.; Fuller, W.; Mackerron, D. H.; Harvie, J. L.; Oldman, R. J.; Riekel, C. Polymer 2000, 41, 7793.
24. Mahendrasingam, A.; Blundell, D. J.; Marian, C.; Fuller, W.; Mackerron, D. H.; Harvie, J. L.; Oldman, R. J.; Riekel, C. Polymer 2000, 41, 7803.
25. Mahendrasingam, A.; Blundell, D. J.; K. Wright, A.; Urban, V.; Narayanan, T.; Fuller, W. Polymer 2003, 44, 5915.
26. Middleton, A. C.; Duckett, R. A.; Ward, I. M.; Mahendrasingam, A.; Martin, C. J. Appl. Polym. Sci. 2001, 79, 1825.
27. Blundell, D. J.; Eeckhant, G.; Fuller, W.; Mahendrasingam, A.; Martin, C. Polymer 2002, 43, 5197.
28. Keum, J. K.; Kim, J.; M. Lee, S.; Song, H. H.; Son, Y. K.; Choi, J. I.; Im, S. S. Macromolecules 2003, 36, 9873.
29. Welsh, G. E.; Blundell, D. J.; Windle, A. H. Macromolecules 1998, 31, 7562.
30. Welsh, G. E.; Blundell, D. J.; Windle, A. H. J. Mater. Sci. 2000, 35, 5225.
31. Kawakami, D.; Ran, S.; Burger, C.; Fu, B.; Sics, I.; Chu, B.; Hsiao, B. S. Macromolecules 2003, 36, 9275.
32. Kawakami, D.; Hsiao, B. S.; Ran, S.; Burger, C.; Fu, B.; Sics, I.; Chu, B.; Kikutani, T. Polymer 2004, 45, 905.
33. Hsiao, B. S.; Kennedy, A. D.; Leach, R. A.; Cho, B.; Harney, P. J. Appl. Cryst. 1997, 30, 1084.

34. Ran, S.; Zong, X.; Fang, D.; Hsiao, B. S.; Chu, B.; Ross, R. J. Appl. Cryst. 2000, 33, 1031.
35. Wu. J.; Schultz, J. M.; Samon, J. M.; B. Pangelinan, A.; H. Chuah, H. Polymer 2001, 42, 7161.
36. Wu. J.; Schultz, J. M.; Samon, J. M.; B. Pangelinan, A.; H. Chuah, H. Polymer 2001, 42, 7141.
37. Okumura, W.; Yamaguchi, T.; Ohkoshi, Y.; Gotoh, Y.; Nagura, M. Intern. Polym. Proc. 2002, 17, 2, 124.
38. Okumura, W.; Kanegae, T.; Ohkoshi, Y.; Gotoh, Y.; Nagura, M. Intern. Polym. Proc. 2003, 18, 46.
39. Okumura, W.; Ohkoshi, Y.; Gotoh, Y.; Nagura, M.; Urakawa H.; Kajiwara, K. J. Polym. Sci., Polym. Phys., 2004, 42, 79.
40. Okumura, W.; Ohkoshi, Y.; Gotoh, Y.; Nagura, M. J. Polym. Sci., Polym. Phys., 2003, 41, 2322.
41. Uddin, A. J.; Ohkoshi, Y.; Gotoh, Y.; Nagura, M.; Endo, R.; Hara, T. J. Polym. Sci., Polym. Phys., 2004, 42, 433.
42. Ikaga, T.; Ohkoshi, Y.; Gotoh, Y.; Nagura, M.; Kawahara, Y. SEN'I GAKKAISHI, 59, 235 - 238, 2003.
43. Ikaga, T.; Kobayashi, A.; Ohkoshi, Y.; Gotoh, Y.; Nagura, M.; Urakawa H.; Kajiwara, K. SEN'I GAKKAISHI, 58, 8 - 15, 2002.
44. Ikaga, T.; Kobayashi, A.; Ohkoshi, Y.; Gotoh, Y.; Nagura, M. SEN'I GAKKAISHI, 58, 16 - 21, 2002.

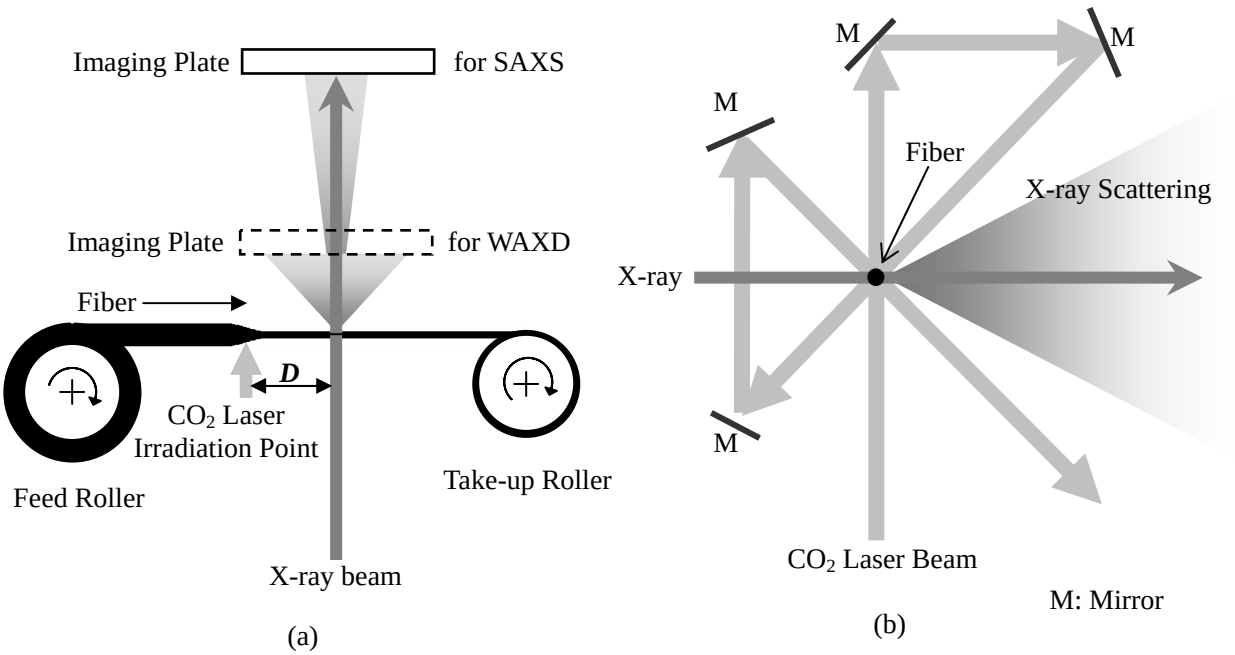

Fig. 1 Schematic diagram of in-situ x-ray scattering measuring system; top view of the system (a) and the CO_2 laser irradiation system (b). As shown in (b), CO_2 laser beam is irradiated three times from three different directions perpendicular to the running fiber. The CO_2 laser irradiation system can move along the running fiber. And the *D* noted in (a) indicates a distance between the laser beam irradiation point and the x-ray beam irradiation point.

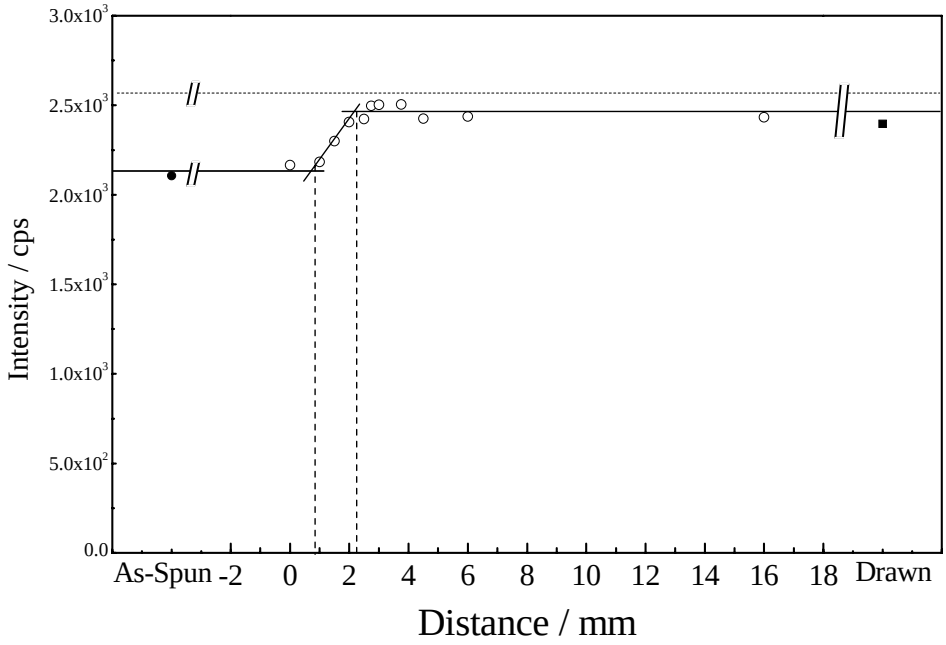

Fig. 2 Averaged transmitted x-ray intensity measured during SAXS measurement. The horizontal axis represents the distance *D* shown in fig. 1 (a).

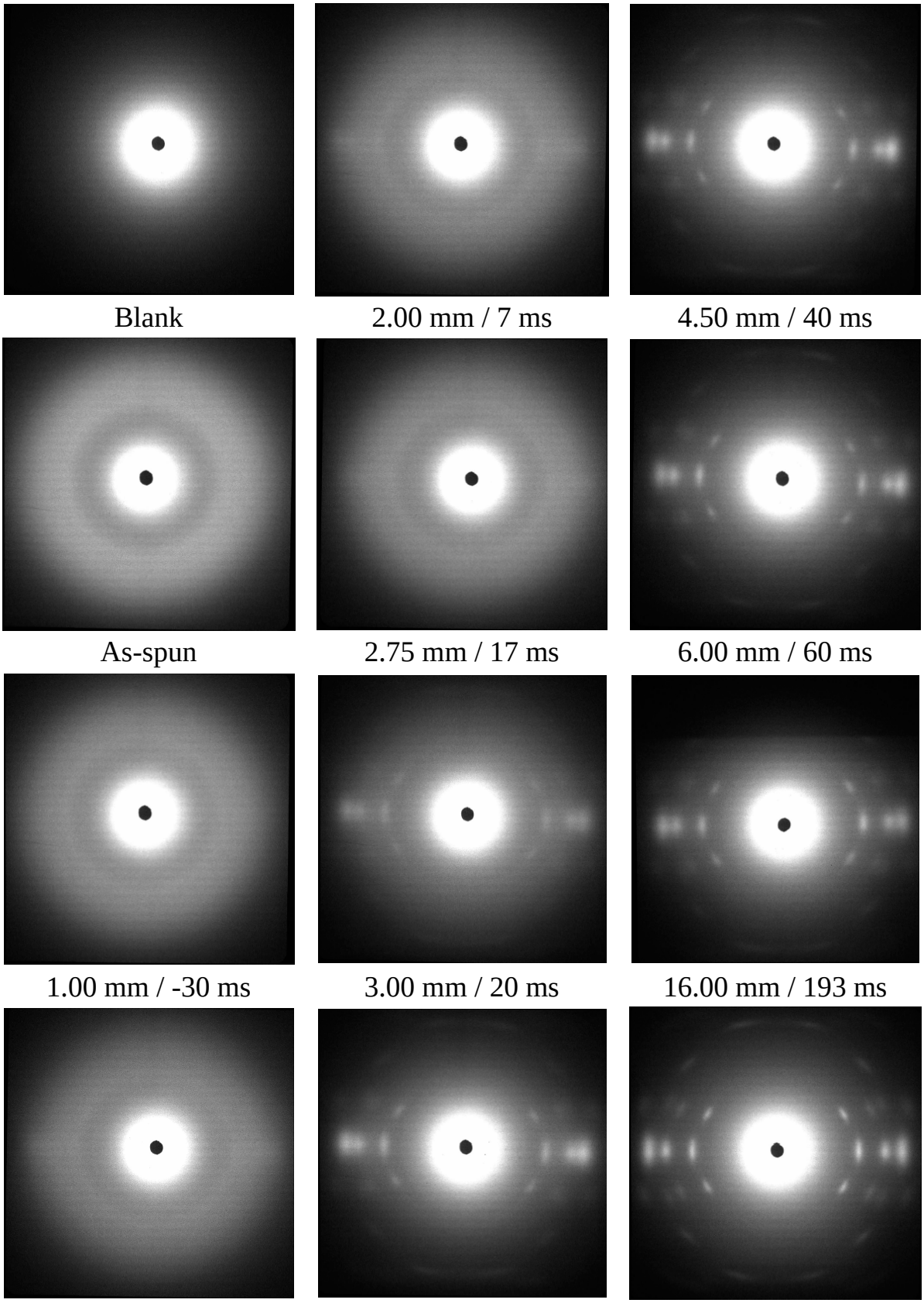

Fig. 3 WAXD images; distance *D* and estimated time after necking are noted in the figure.

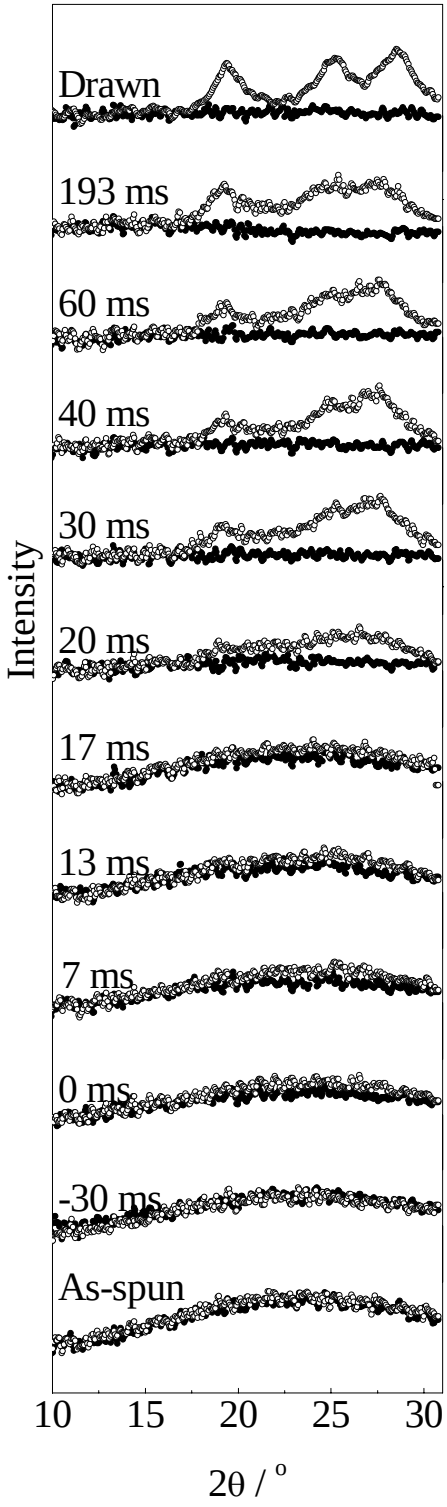

Fig. 4 Equatorial and meridian WAXD profiles; estimated time after necking are noted in the figure. Equatorial profiles (○), meridian profiles (●).

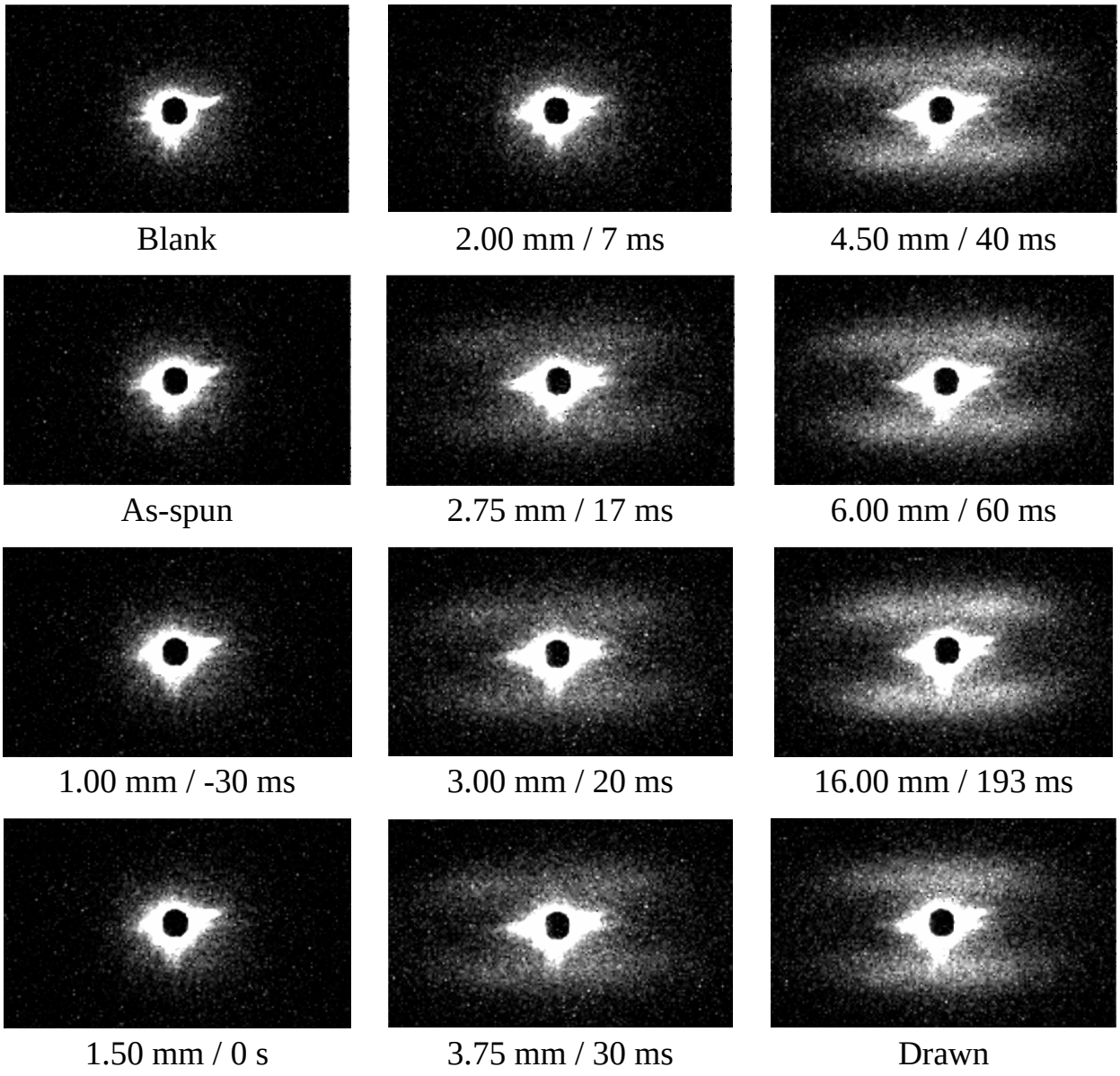

Fig. 5 SAXS images; distance *D* and estimated time after necking are noted in the figure.

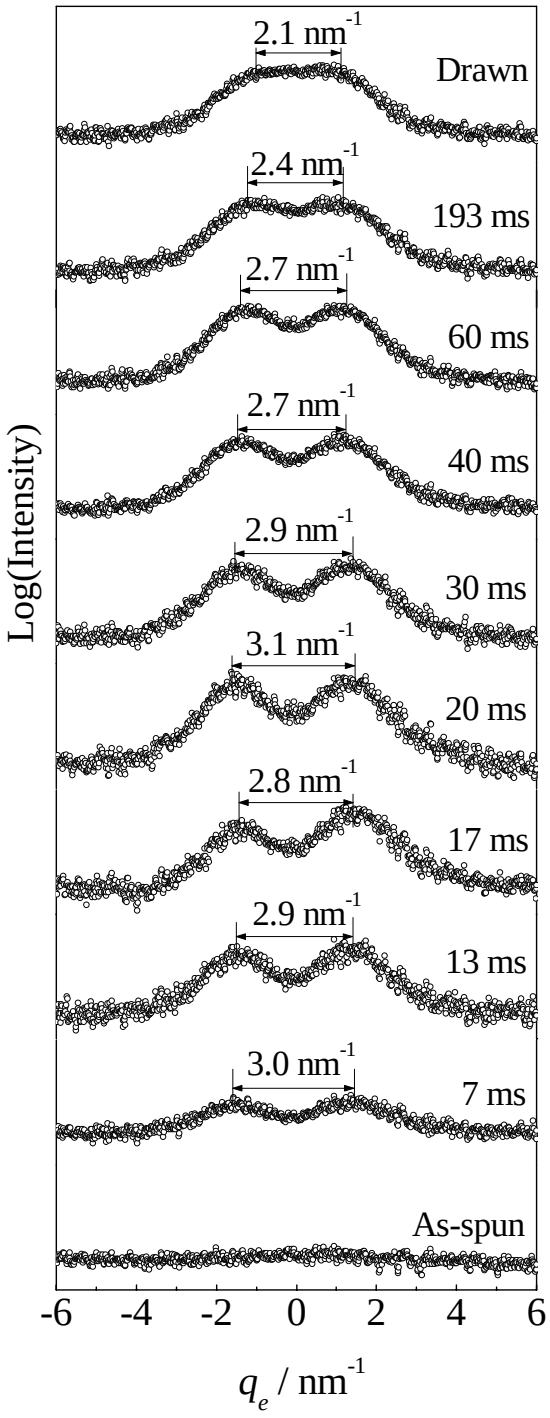

Fig. 6 Equatorial SAXS profiles obtained by integrating q_m of image from 0.66 nm^{-1} to 1.19 nm^{-1}; estimated time after necking are noted in the figure. Peak separations are noted in the figure.

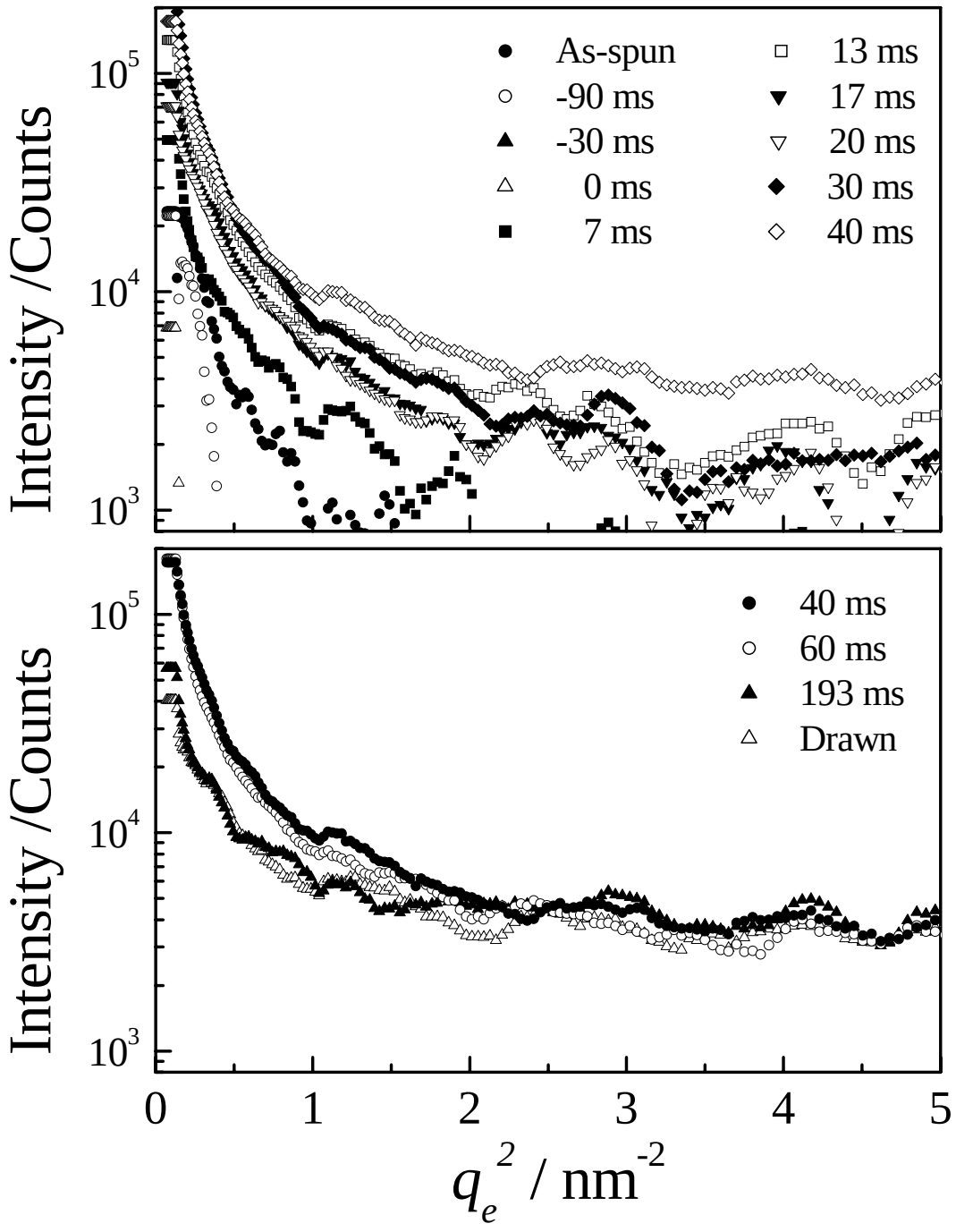

Fig. 7 Equatorial SAXS profiles; estimated time after necking are noted in the figure.